ACS APPLIED MATERIALS & INTERFACES



Article

# Ultrasensitive and Selective Organic FET-type Non-enzymatic Dopamine Sensor Based on Platinum Nanoparticles Decorated Reduced Graphene Oxide

Jungkyun Oh, Jun Seop Lee, Jaemoon Jun, Sung Gun Kim, and Jyongsik Jang

*ACS Appl. Mater. Interfaces*, **Just Accepted Manuscript** • DOI: 10.1021/acsami.7b15093 • Publication Date (Web): 25 Oct 2017



## Just Accepted



ACS Publications

ACS Applied Materials & Interfaces is published by the American Chemical Society.
1155 Sixteenth Street N.W., Washington, DC 20036

# Ultrasensitive and Selective Organic FET-type Non-enzymatic Dopamine Sensor Based on Platinum Nanoparticles Decorated Reduced Graphene Oxide

*Jungkyun Oh, Jun Seop Lee, Jaemoon Jun, Sung Gun Kim and Jyongsik Jang**

School of Chemical and Biological Engineering, College of Engineering, Seoul National University (SNU), 599 Gwanangno, Gwanak-gu, Seoul, 151-742 (korea)

†Tel: 82-2-880-8348; Fax: +82-2-888-7295; e-mail: jsjang@plaza.snu.ac.kr

## ABSTRACT

Dopamine (DA), a catecholamine hormone, is an important neurotransmitter that controls renal and cardiovascular organizations and regulates physiological activities. Abnormal concentrations of DA cause unfavorable neuronal illnesses such as Parkinson's disease, schizophrenia, and attention deficit hyperactivity disorder (ADHD)/attention deficit disorder (ADD). However, the DA concentration is exceedingly low in patients and difficult to detect with existing biosensors. In this study, we developed an organic field-effect-transistor-type (OFET) non-enzyme biosensor using platinum nanoparticles decorated reduced graphene oxide (Pt_rGO) for ultrasensitive and selective DA detection. The Pt_rGOs were fabricated by reducing GO aqueous solution containing Pt precursors (PtCl4) with a chemical reducing agent. The Pt_rGOs were immobilized on graphene substrate by π–π interactions and a conducting-polymer source–drain electrode was patterned on the substrate to form the DA sensor. The resulting OFET sensor showed a high sensitivity to remarkably low DA concentrations ($100 \times 10^{-18}$ M) and selectivity among interfering molecules. Good stability was expected for the OFET sensor, because it was fabricated without an enzymatic receptor, and π–π conjugation is part of immobilization process. Furthermore, the OFET sensors are flexible and offer the possibility of wide application as wearable and portable sensors.



**KEYWORDS**

Dopamine; electrochemical sensor; field-effect-transistor; reduced graphene oxide; wearable sensor; portable sensor.

## BRIEFS

A non-enzymatic organic field-effect-transistor sensor was fabricated using platinum nanoparticles decorated reduced graphene oxide sheet (Pt_rGO). This robust and flexible sensor detected dopamine selectively and with high sensitivity.

# INTRODUCTION

Dopamine (DA), a neurotransmitter, has been extensively studied because it plays an important role in the renal, hormonal, and cardiovascular systems and regulates numerous physiological activities. Abnormal levels of DA are related to certain neurological disorders such as Parkinson's disease, drug addiction, and schizophrenia.[1-5] Clinically, detection of low DA concentration is essential because the DA concentration in urine, plasma, and single adrenal chromaffin cells are in the range of $10^{-6}$ M, $10^{-9}$ M and $10^{-15}$ M, respectively. Therefore, several quantitative analytical methods have been developed to detect DA for purpose of cellular investigations and biomedical diagnosis. High-performance liquid chromatography (HPLC) and mass spectroscopy have very low DA detection limits.[6, 7] However, these methods are inexpensive, and they require sample pretreatments and special instrumentation. Enzymatic-assay-based methods have also attracted considerable attention due to their high sensitivity and comparative low cost.[8, 9] Despite these advantages, these methods are not commonly used due to their low stability and complicated process to attach enzyme to transducer. Therefore, a simple analytical method is needed for DA detection that offers high sensitivity, and high target selectivity.

New electrochemical methods have been developed to detect low DA concentrations. Notably, field effect transistor (FET) based sensor has the advantages of miniaturization, simple operation, fast response, reliability, and high sensitivity to the target analyte.[10-15] These characteristics are useful for diagnoses at the early stages of diseases. However, fabrication of source–drain electrode for the FET-type sensor requires several complex and time-consuming processes such as photolithography and thermal vapor deposition used to pattern the gold source–drain electrode on the substrate surface.[16-20] Hence, electrode patterning using a conducting polymer (CP) is attractive, due to its cost effectiveness and

facile fabrication method.[21-25] CP electrode based sensors have as high sensing performances as gold-patterned FET-type sensors, and have many potential applications in portable or wearable electronic devices. They also exhibit great promise for chemical and biological sensor applications.[26-29]

Solution-processed CPs have been anticipated as materials for flexible devices due to facile synthesis, high electrical conductivity, and various morphologies with diverse substrates.[30, 31] Especially, PANI:CSA has been greatly expected as a material for flexible devices because of its high electrical conductivity and excellent free-processiblity with organic solvents. In particular, the solution-processed PANI:CSA displays $10^2$ to $10^3$ higher electrical conductivity than pristine PANI powder without doping due to change of polymer chain conformation with bonding to CSA in the organic solvent.[32] As a result, the coil conformation of the PANI chains becomes more expanded that leads to elevated electrical conductivity of the PANI.[33]

Recently, various inorganic nanocomposites have been decorated on graphene sheets. For example, graphene sheet decorated with metal nanocomposites has been used in fuel cells, batteries, and transducers for sensors, because their electrical and semiconducting properties were greatly improved over pristine metals or graphene alone.[34-37] This behavior was attributed to the metal composites preventing aggregation of the graphene sheets and improved electron transport.[38]

Herein, we suggest the fabrication of an organic FET-type (OFET) non-enzymatic biosensor to detect DA. Water-stable p-channel semiconductor, Pt_rGO, was fabricated as the DA detection material by a chemical reduction. The Pt_rGO solution was easily attached on a substrate using spin-coating, and the source–drain electrode pattern was screen-printed onto the DA detecting layer with a CP to fabricate the sensor. For widespread use as a DA sensor,

the detection level must be as low as $10^{-15}$ M. Our sensor demonstrated enhanced sensitivity to DA at the low concentration of $10^{-16}$ M and displayed high selectivity to the target analyte in the presence of interfering molecules, such as uric acid (UA), ascorbic acid (AA), epinephrine (EP), and norepinephrine (NE). Our DA sensor has a longer lifetime than that of aptamer-attached biosensors. Furthermore, its flexibility offers the possibility of wearable and portable sensors.

## RESULTS AND DISCUSSION

### Fabrication of the OFET-type Non-enzymatic DA Sensor.

**Figure 1** schematically illustrates a Pt_rGO based OFET sensor configuration. Large-scale graphene was synthesized by chemical vapor deposition (CVD) method and transferred to a poly(ethylene naphthalene) (PEN) substrate for flexibility.[39] Furthermore, a large-area graphene sheet was fabricated by CVD with the object of immobilizing the Pt_rGO substrate. The transducer materials could be immobilized on the sensor substrate to improve stability by the π–π conjugation of the resonance structures of carbon rings. The stability in the liquid-ion solution was one of the critical factors in the fabrication of the ultrasensitive FET biosensor electrodes. **Figure S1** shows a TEM image of the CVD graphene surface and a HR-TEM image of the CVD graphene layer. The HR-TEM image of **Figure S1** reveals that two-layer graphene sheets were created by the CVD process.

The Pt_rGO aqueous solution was spin-coated on the large area graphene sheet to form a stable and homogeneous receptor layer for highly sensitive analyte adsorption. The Pt_rGO component was anchored on the CVD graphene without any surface treatment by π–π stacking between the carbon rings of Pt_rGO and the plane of graphene. **Figure 2** illustrates the decoration of platinum (Pt) nanoparticles on the rGO surface by chemical reduction process. The Pt cations were adsorbed onto the GO surface as a result of the charge–charge interactions between the positive charge of the Pt cations and the partial negative charge of the oxygen atoms in the GO structure.[40,41] The reducing agent ($NaBH_4$) was added to the aqueous solution to concurrently transform the $Pt^{4+}$ to $Pt^0$ and the GO to rGO to form Pt decorated rGO (Pt_rGO), **Figure 3a**. **Figure 3b** shows HR-TEM images of Pt_rGO interplanar spacings between the noble metal nanoparticles of 0.2 and 0.23 nm diameters for the [200] and [111] planes, respectively, according to the Pt FCC lattice structure. **Figure S2**

shows TEM images of GO sheet and the density of the Pt nanoparticles on rGO, controlled by the concentration of $PtCl_4$ aqueous solution. Each Pt_rGO obtained 4.0-4.5 nm Pt nanoparticle radii and were labeled with different densities of Pt nanoparticles as Pt_rGO_0.5 (**Figure S2b**), Pt_rGO_2.5 (**Figure S2c**), and Pt_rGO_5.0 (**Figure 3a**), respectively. The aggregation of Pt nanoparticles was appeared on the surface of rGO when the concentration of $PtCl_4$ aqueous solution exceeded $5.0 \times 10^{-4}$ M, **Figure S2d**.

For further understanding, element analysis methods were used and **Figure S3** showed the results. **Figure S3a** shows the X-ray diffraction (XRD) patterns of GO and Pt_rGO_5.0. The result confirmed that the platinum precursor was reduced well by the reducing agent ($NaBH_4$). Raman spectroscopy was used to analyze the structure and quality of the carbonaceous materials, as shown in **Figure S3b**. The result suggested that GO was partially reduced. Under our experimental condition, sensing nanomaterials require semiconducting ability, and partially reduced GO sheets were suitable for our research. XPS characterization, **Figure S3c-f**, was used to analyze the elemental composition of the hybrid nanomaterials. The XPS spectrum of pristine GO revealed only the presence of C and O atoms, while the spectrum of Pt_rGO_5.0 expressed the presence of C, O and Pt atoms. The presence of Pt atoms in the Pt_rGO_5.0 spectrum indicated that Pt nanoparticles had been deposited onto the surface of the rGO. Also, the Pt 4f high-resolution spectrum of Pt_rGO_5.0 was exhibited in **Figure S3f**.

**Figure S4a** depicted a schematic diagram of the OFET and **Figure S4b** presented a FE-SEM image of the Pt_rGO attached graphene sheet. A source–drain electrode pattern was screen-printed on the surface of the Pt_rGO immobilized CVD graphene sheet using PANI:CSA. The PANI:CSA also adhered to the Pt_rGO immobilized CVD graphene surface due to π–π stacking between the carbon rings of the components. The real device was presented in **Figure 4a**. Also, the enlarged sensing part of device was demonstrated in **Figure**

**4b**. In **Figure 4b**, solution-processed PANI:CSA, screen-printed on the surface of Pt_rGO attached CVD graphene, had no blur effect due to suitable viscosity for patterning and π–π stacking between the carbon rings of the components. Spin-coated Pt_rGO sheets, dopamine sensing materials, covered the gap between branch-shaped PANI:CSA electrodes and connected them. As a result, this device could work as dopamine sensing device in PBS solution phase. Additional details of the fabrication process are noted in the Materials and Methods Section.

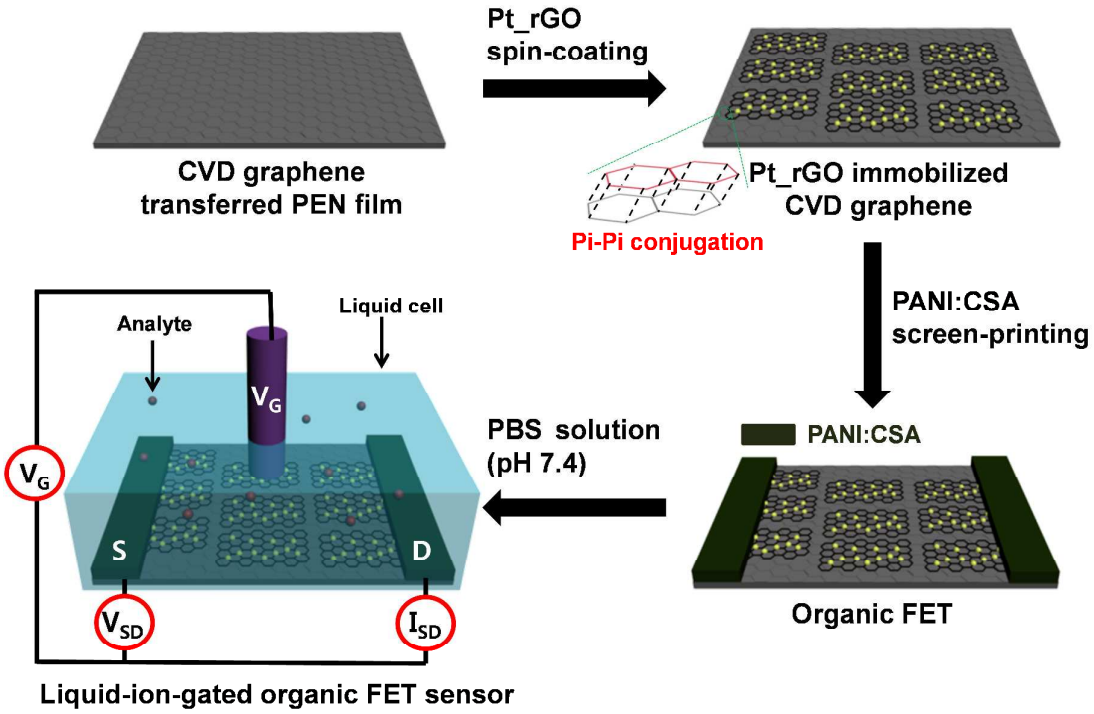


**Figure 1.** Illustrative diagram of the sequence of steps for the fabrication of the organic field-effect-transistor-type (OFET) sensor using chemical vapor deposition (CVD) graphene, polyaniline:camphorsulfonic acid (PANI:CSA) and Pt decorated reduced graphene oxide (Pt_rGO).

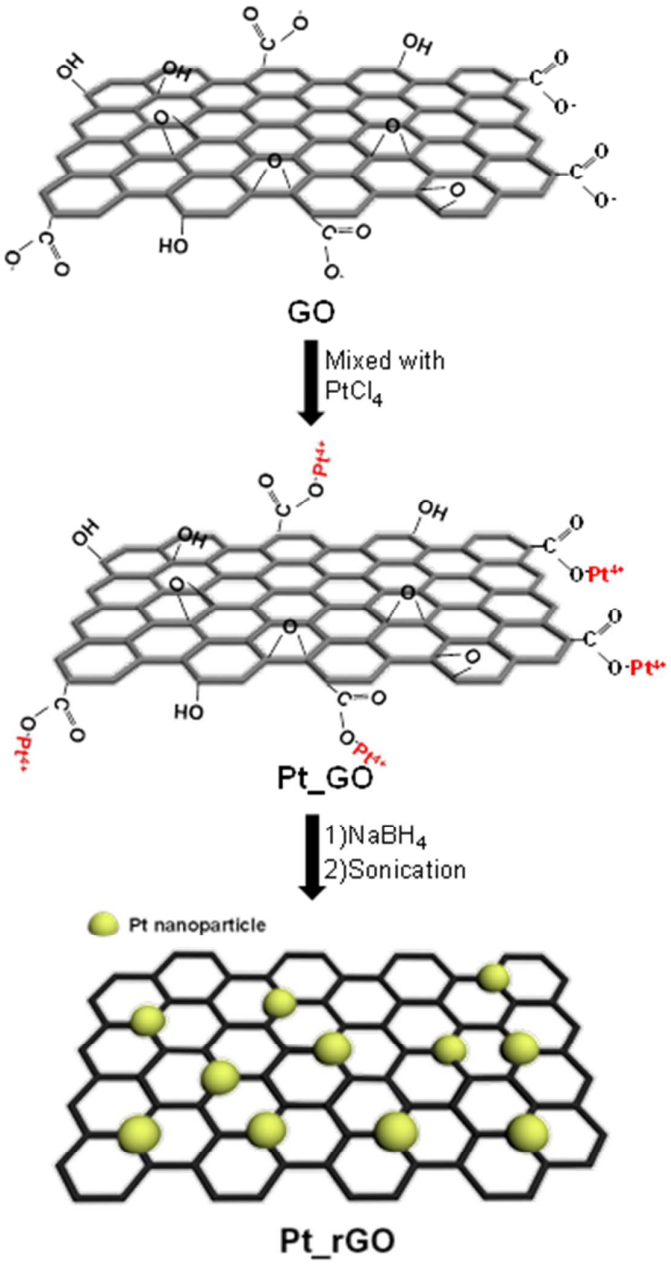


**Figure 2.** Schematic diagram of the fabrication steps for the Pt nanoparticle decorated reduced graphene oxide (Pt_rGO).

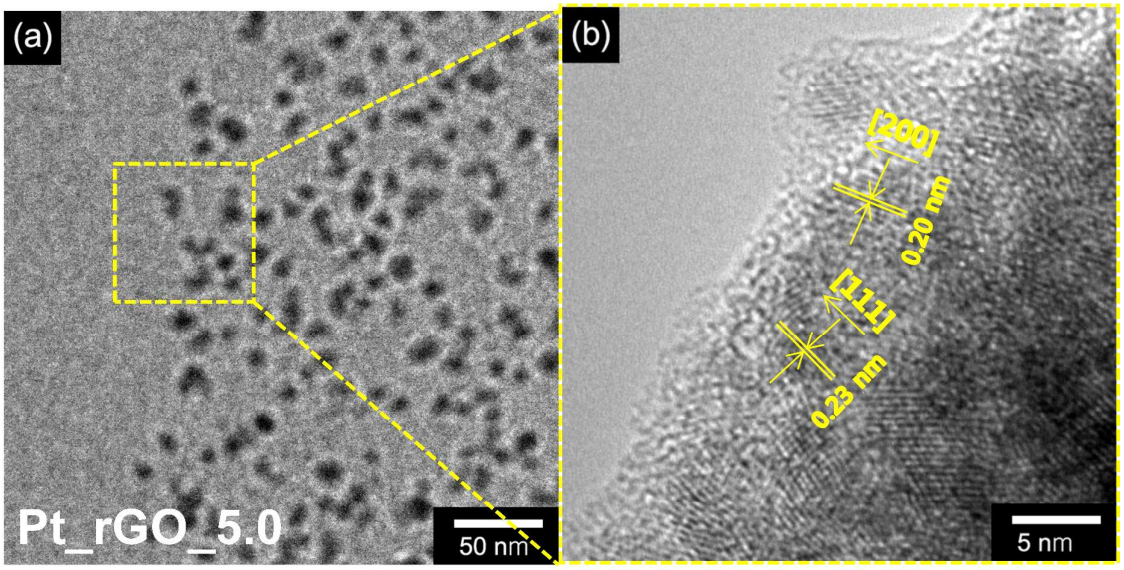


**Figure 3.** (a) TEM and (b) HR-TEM images of the Pt_rGO_5.0 sheet.

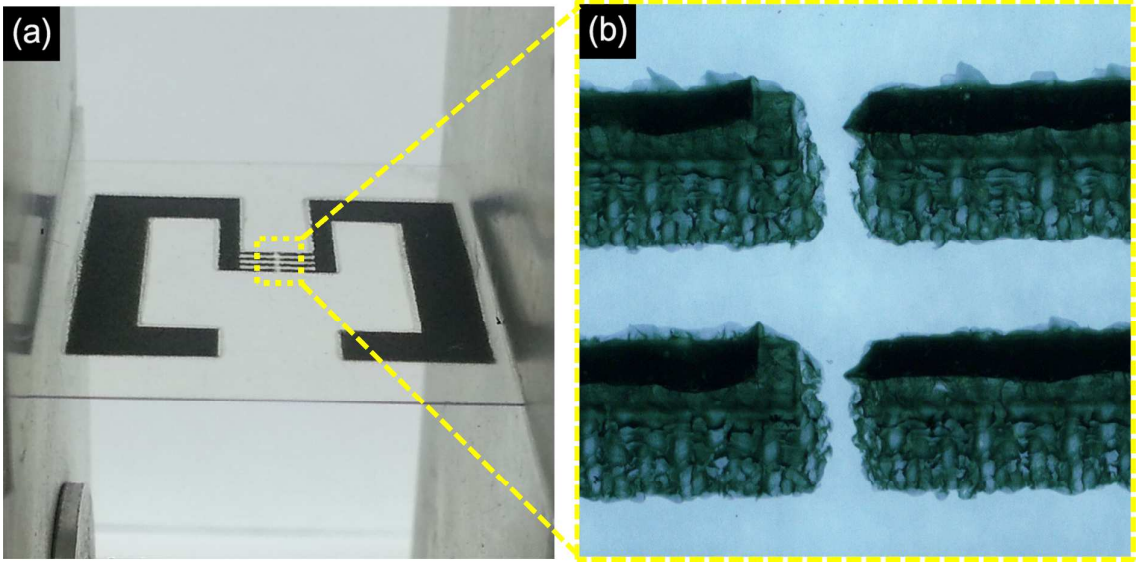


**Figure 4.** Photographs of (a) OFET dopamine sensor device and (b) enlarged sensing part of device.

**Characterization of the OFET-type Non-enzymatic DA Sensor.**

To characterize electrical properties of Pt_rGOs in liquid phase, electrolyte was used as liquid-ion gate in the OFET configuration. The liquid-ion gate is capable of achieving increased transconductance, owing to the intimate contact between the NPs and the gate, compared with conventional back-gating.[42] Current–voltage (*I–V*) curves were analyzed to estimate the electrical contact of Pt_rGOs on the large-scale CVD graphene surface. **Figure 5a** shows the $I_{SD}$-$V_{SD}$ properties of each Pt_rGO made different Pt nanoparticle populations for the case of $V_G = 0$. The curves were linear form for voltage from –0.1 V to 0.1 V and then the *dI/dV* value increased with growing numbers of Pt nanoparticles on the rGO surface. According to the results, Pt nanoparticles enhanced the conductivity of the rGO sheets (**Figure S5**). The feasibility of flexible device was also confirmed by current-voltage *(I-V)* curves at $V_G = 0$. DA sensor device was folded for 100 times by folding machine (**Figure S6**) and the $I_{SD}$-$V_{SD}$ properties of each Pt_rGO, made by different Pt nanoparticle populations, was re-measured for the case of $V_G = 0$. There were just little differences of the Pt_rGO *dI/dV* values after 100 times folding. Furthermore, the influence of folding was decrease with growing numbers of Pt nanoparticels on the rGO surface. As a result, folding process gave no influence to conductivity of Pt_rGO sheets and it showed the possibility for flexible and portable sensor. Moreover, the source–drain current ($I_{SD}$) for various $V_G$s at a constant scan rate of 100 $mV \cdot s^{-1}$ of source–drain voltage ($V_{SD}$) validated the charge transport characteristics of Pt_rGOs in OFET configuration. **Figure 6** exhibits $I_{SD}$–$V_{SD}$ plots for various $V_G$s for Pt_rGO sheets with different amount of Pt nanoparticles. The source–drain current ($I_{SD}$) was negatively increased with negatively increasing $V_G$, signifying a p-type property for the Pt_rGO; this semiconductor was attributed to hole-transport caused by an increase in the oxidation level of the rGO chains of Pt_rGO. In **Figure 6**, increase of Pt nanoparticles

amount on rGO sheet demonstrated demolition of p-type charge transport properties in the FET configuration since Pt nanoparticles limited semiconductance of rGO sheets. However, the function of p-type semiconductance was still maintained and it was showed well in **Figure 6c**. The analysis of the dependence of $I_{SD}$ on $V_G$ suggested that a Pt_rGO based OFET could function as an electrochemical sensor for the detection of specific analytes in the liquid phase.

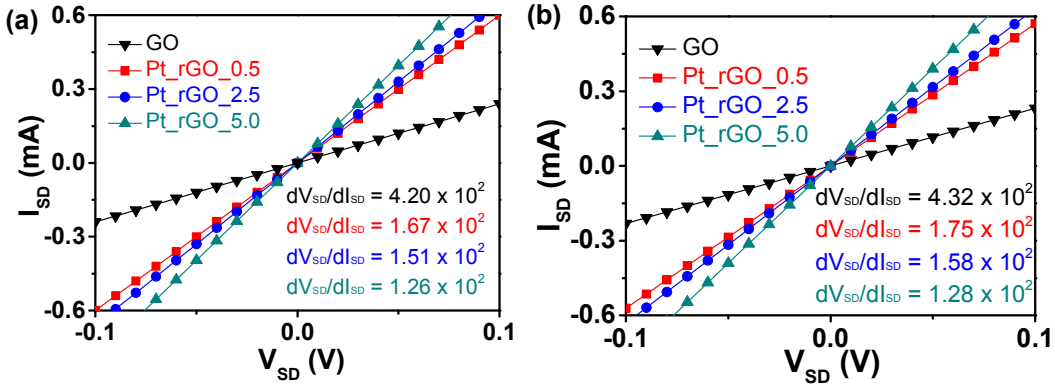


**Figure 5.** (a) Source–drain current-voltage ($I_{SD}$–$V_{SD}$) curves of OFETs with different Pt_rGOs without a gate potential voltage ($V_G$) before folding. (b) Source–drain current-voltage ($I_{SD}$–$V_{SD}$) curves of OFETs with different Pt_rGOs without a gate potential voltage ($V_G$) after folding for 100 times.

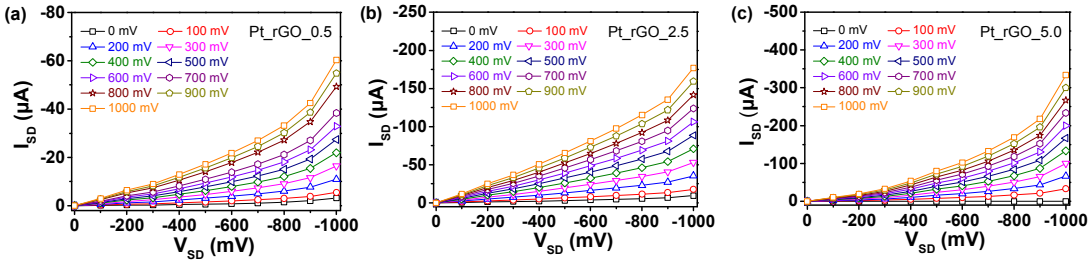


**Figure 6.** Source–drain current-voltage ($I_{SD}$–$V_{SD}$) curves of (a) Pt_rGO_0.5, (b) Pt_rGO_2.5 and (c) Pt_rGO_5.0 OFET electrodes for variable gate voltages ($V_G$) ranging from 0 mV to 1000 mV in 100 mV steps.

**Real-time Response of the OFET-type Non-enzymatic DA Sensor.**

The Pt_rGOs uniformly immobilized on the OFET sensor surface rapidly detected DA at room temperature via charge transfer of electrons. While DA aqueous solution was injected into PBS solution, DA molecules were attached to surface of Pt_rGO due to π-π interactions between benzene rings of rGO and DA molecule.[43-47] The catalytic effect of Pt nanoparticles oxidized DA molecules to dopamine-o-quinone (DQ) molecules. At this time, 2 hydrogen atoms and 2 electrons were released simultaneously from each DA molecule and released electrons transferred to rGO. The illustrative diagram of dopamine detecting mechanism was demonstrated in **Figure S7**. Because rGO acts as a p-type transducer, number of holes in rGO structure was decreased and $I_{SD}$ was also diminished through this property. To measure the sensing ability of an OFET sensor, the change in current as a function of DA concentration was observed in real time at constant $V_G$ (1 V) and $V_{SD}$ (10 mV). **Figure 7a** describes the real-time responses of the OFET sensors as a function of DA concentrations for different amounts of Pt nanoparticles decorated on rGO. The OFET sensor showed a rapid real-time response (<1 s) to the target and exhibited a concentration dependent reduction in the $I_{SD}$ on exposure to different analyte concentrations. The sensitivity of the OFET sensor improved with increasing amounts and radius of Pt nanoparticles on the rGO surface. The increment of number and radius of Pt nanoparticles on the rGO surface increased the surface area of Pt_rGOs. We calculated the surface area of rGO, Pt_rGO_2.5 and Pt_rGO_5.0 by Brunauer-Emmet-Teller (BET) instrument and it was resulted as 13.6806 $m^2 \cdot g^{-1}$, 25.1363 $m^2 \cdot g^{-1}$ and 47.7263 $m^2 \cdot g^{-1}$, respectively (**Figure S8**). Because larger surface area gave more chance to DA to contact with Pt_rGO, the catalytic activity toward oxidizing DA molecules was increased with increasing surface area. Since greater numbers and radius of Pt nanoparticles displayed better catalytic activity toward oxidizing DA molecules, the sensing ability to DA

molecules also increased in the same manner. Hence, the OFETs, made from Pt_rGO_0.5, Pt_rGO_2.5, and Pt_rGO_5.0, were capable of detecting DA concentrations as low as $10^{-12}$ M, $10^{-14}$ M and $10^{-16}$ M at room temperature, respectively. **Figure 7b** exhibits the calibration curve for the detection ability of the OFET sensor. The sensitivity (S) symbolizes the normalized current changes ($\Delta I/I_0 \times 100$) measured after analyte particles were injected. The Pt_rGO with the most Pt nanoparticles suggested the highest sensitivity over a wide range of DA concentrations. To compare the performance of liquid-ion gate sensor device with conventional method, back-gate DA sensing device was manufactured and DA sensing test was performed with it. Schematic diagram of back-gate DA sensing device was appeared in **Figure S10a**. Pt_rGO_5.0, the best performed sensing material, was used as sensing material for back gate sensing device. As a result, it showed same detection limit with liquid-ion gate in **Figure S10b**. However, the current changes of back gate sensing were smaller than liquid-ion gate and the signals with high concentration were unstable. Also, saturation was appeared faster than liquid-ion gate at $10^{-4}$M. This phenomenon was caused because the liquid-ion gate is capable of achieving more increased transconductance than back-gating, as mentioned above.

The selectivity of the OFET sensor to DA was investigated (**Figure 8a**). Six different organic molecules (tyrosine (TR), phenethylamine (PEA), uric acid (UA), ascorbic acid (AA), norepinephrine (NE), and epinephrine (EP)) were chosen as non-target molecules for the sensor. NE and EP were selected due to their similar molecular structures to DA. UA and AA were chosen because these molecules appear with DA in some animal tissues. TR and PEA were selected owing to not only their like molecular structures to DA, but also appearance with DA in some animal tissues. The structures of the six organic molecules are illustrated in **Figure S9**. All non-target analytes were injected into the OFET sensor at a concentration of

$10^{-11}$ M. No significant current changes of TR, PEA, AA and UA and small current changes of AA and UA were observed after injection. However, a large change in $I_{SD}$ was detected with $10^{-12}$ M of DA, which indicated a high selectivity to DA molecules by the OFET sensor. AA and UA caused no current changes, due to the absence of phenyl groups in their molecular structures, which led to only weak π–π interactions between the receptor and analyte. Despite their similar structures to DA, TR and TEA also showed no current changes owing to absence of catechol structures which induced catalytic reaction between Pt and analytes. NE and EP presented unimpressive sensitivity to the OFET sensor compare to DA. The side-chains of NE and EP attached to their catechol structures increased their dimensions to longer than that of the DA chain. Consequently, the increased size of these biomolecules reduced the effects of π–π interactions and catalytic activities of the Pt nanoparticles. **Figure 8b** shows the outstanding change in signal observed for DA in a solution of analytes consisting of a mixture of 1 pM of each of the six non-target organic molecules. The same concentration of DA solution was added to the mixture. There was insignificant difference between the size of the signal for 1 pM of DA present in the mixture (**Figure 8b**) and alone (**Figure 7a**).

Clearly, the interferents did not affect the OFET sensor and did not affect its ability to detect DA molecules. **Table S1** presents the optimal analytical characteristics of the OFET sensor; details of other electrochemical sensors are also listed. The OFET sensor demonstrated impressive analytical performance: better selectivity, faster response time, wider linear range and a lower detection limit than other electrochemical sensors reported to date.

**Figure 9a** depicts the response changes of the OFET sensor after repeated folding and relaxing sequences. The detailed experimental process is illustrated in **Figure S6**. Flexibility

is important for biosensor development, because the development of flexible, portable, or wearable sensors has proven particularly challenging. After 1000 cycles of repeated folding and relaxing, the performance of the OFET sensor was diminished by less than 5%. This result clearly indicates the excellent flexibility and durability of the OFET sensor and suggests the feasibility of manufacturing flexible biosensors. **Figure 9b** illustrates the stability over several weeks of OFET sensors having various Pt densities provided by Pt_rGOs. Good sensor stability is especially important. To confirm the reusability of an OFET sensor, the same OFET electrode was used every week to detect DA at a constant concentration of $10^{-12}$ M. Washing and rinsing of the electrode was repeated several times to eliminate any residue on the OFET sensor after a sensing test. **Figure 9b** shows that the sensor maintained its sensitivity over four weeks; this was attributed to two key factors. First, the organization of the OFET sensor did not require enzymatic bioreceptors to detect the biomolecules. The structure of a bioreceptor is easily transformed by environmental changes, and a biosensor containing a bioreceptor is usually inactivated by harsh conditions. However, the OFET sensor based on Pt_rGOs preserved its sensing performance under various circumstances. Second, π–π bonds between CVD graphene and the rGOs maintained the constitution of the OFET sensor. Other sensing performance indicators, such as selectivity and minimum detectable level (MDL), were also maintained for the reasons mentioned above.

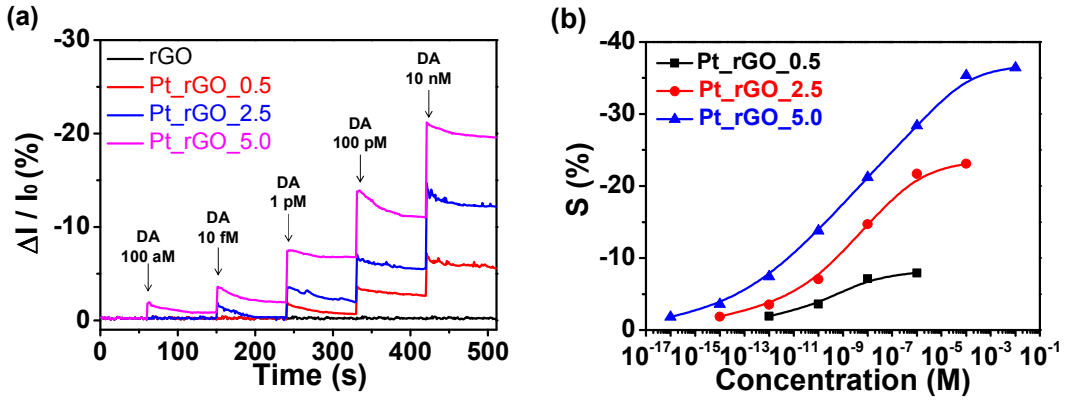


**Figure 7.** (a) Real-time responses of the different OFETs to various dopamine concentrations comprising effects of Pt nanoparticle densities of Pt_rGOs, with normalized current changes ($\Delta I/I_0 = (I - I_0)/I_0$, where $I_0$ is the initial current and $I$ is the instantaneous current). (b) Calibration curves of OFETs comprising various Pt nanoparticle densities of Pt_rGOs (S signifies the normalized current changes).

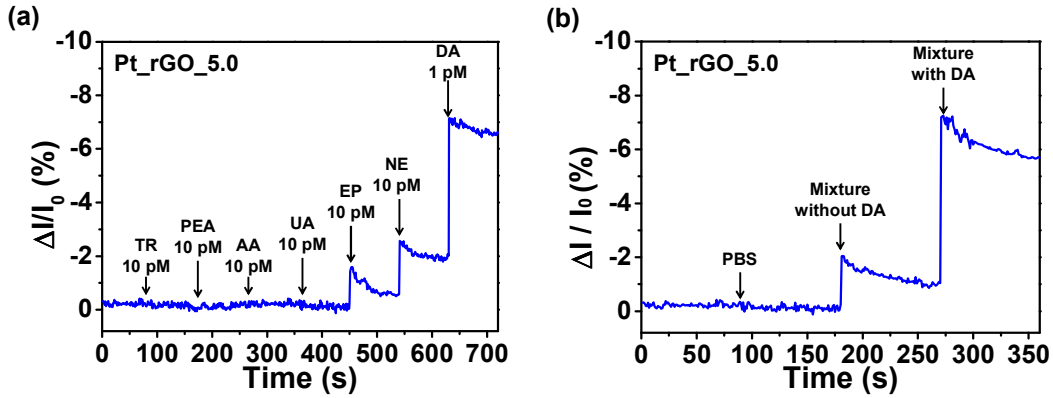


**Figure 8.** (a) Real-time responses of OFET biosensor to target (dopamine (DA)) and non-target (tyrosine (TR), phenethylamine (PEA), ascorbic acid (AA), uric acid (UA), epinephrine (EP), norepinephrine (NE)) analytes. (b) Real-time responses of OFET non-enzyme biosensor for variable analytes (Analytes were phosphate buffer saline (PBS), mixture without DA, mixture with DA).

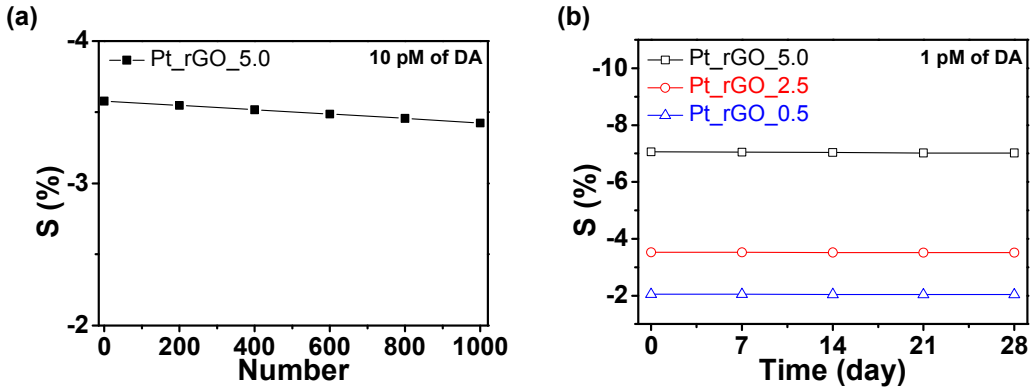


**Figure 9.** (a) Sensing performance of the OFET biosensor formed with Pt_rGO_5.0 after a large number of bending cycles. Measurements were obtained after every 200 cycles. (b) Sensing performance of various OFET DA sensors at one-week intervals over four weeks.

## CONCLUSIONS

In summary, Pt_rGO based OFET sensors with a conducting polymer-patterned electrode were readily fabricated using screen-printing methods. This approach did not require any chemical surface treatments of the components. The Pt_rGOs were produced by a chemical reduction process. The density of Pt nanoparticles decorated on rGOs intensified the oxidation of DA, thereby increasing the sensitivity of the OFET sensor to DA. The OFET sensor exhibited extremely high sensitivity to DA concentration, i.e., $10^{-16}$ M. To our best knowledge, this concentration is $10^3 – 10^4$ times higher than previous researches of other DA sensors. Furthermore, the OFET sensor had equal performance to DA regardless of the presence of interferents. The sensor performed excellent long term stability owing to π–π interactions between the organic components and the absence of an enzymatic receptor on the sensor. The flexibility and performance of the OFET sensor device suggests the possibility of developing flexible, wearable, and portable sensors.

*Supporting Information Available:* The contents of the Supporting Information include the following: (1) TEM images of Pt_rGOs with several concentrations of $PtCl_4$ aqueous solutions; (2) TEM and HR-TEM images of two-layer graphene sheets using chemical vapor deposition; (3) Schematic diagram of OFET and SEM image of Pt_rGO attached graphene surface; (4) Electrical characteristics of GO, rGO and Pt_rGO_5.0; (5) Source–drain current-voltage curves of Pt_rGO_0.5 and Pt_rGO_2.5; (6) Schematic diagram of dopamine detection mechanism of OFET sensors; (7) BET analysis for surface area of rGO hybrid materials; (8) Molecular structures of dopamine and its analogs; (9) Photographs of the OFET dopamine sensor under different formation; (10) Comparison of the Pt_rGOs modified dopamine sensor with other electrochemical detection; This material is available free of charge *via* the Internet at http://pubs.acs.org.

*Acknowledgment.* This work was supported by Development Fund of Seoul National University funded by Dongjin Semichem Co., Korea (0458-20130066).

## MATERIALS AND METHODS

**Materials:** Graphite flake, poly(vinyl alcohol) (PVA, MW 9,000), $FeCl_3$ (97%), aniline (99%), ammonium persulfate (APS, 98.0%), camphorsulfonic acid (CSA, 98%), and sodium borohydride (NaBH4, 99%) were purchased from Aldrich Chemical Company. Platinum (IV) chloride (99%) was acquired from Kojima Chemicals Company. Copper foil (99.8%) was obtained from Alfa Aesar. Ammonia solution ($NH_3$), chloroform ($CHCl_3$), and hydrochloric acid (HCl, 35%) were acquired from Samchun Company. m-Cresol was obtained from Tokyo Chemical Industry which were used as the solvent for the polyaniline:camphorsulfonic acid (PANI:CSA).

**Fabrication of Pt_rGO:** GO was prepared by a modification of the Hummers method. It was dispersed in distilled water at 0.1 wt% and then various concentrations (3 to 30 mmol) of aqueous $PtCl_4$ solution were added. A reducing agent ($NaBH_4$, 5 mmol) was injected into the mixed aqueous solution. Then, the mixture was stirred for 2 h at a suitable temperature to transform the GO into rGO, resulted in Pt_rGO. The solution was sonicated for 2 h using a tip sonicator and dried for sufficient hours to provide Pt_rGO powder.

**Fabrication of the OFET-type Non-enzymatic DA Sensor:** The OFET non-enzymatic DA sensor was fabricated as follows. A large (2 × 2 cm) graphene surface was prepared by chemical vapor deposition (CVD).[39] Aqueous Pt_rGO solution (0.05 wt%) was cast onto the graphene by spin-coating at 500 rpm for 20 s, which formed Pt_rGO adsorbed onto the CVD graphene, and then additionally spun at 1000 rpm for 10 s. The coating was dried in a 60°C oven for several hours. After drying, the source–drain electrode pattern was screen-printed using PANI:CSA, synthesized according to the procedures of Cho et al.[48]

**Electrical Measurement of the OFET-type Non-enzymatic DA Sensor:** All electrical

measurements were measured using Keithley 2612A source meter and probe station (MS TECH, Model 4000) in pH 7.4 of PBS solution. To utilize the solution-based measurement, a glass bath was designed and used. The change in the current was as follows

$$\left[\frac{\Delta I}{I_0}\right]_{SD}(\%)=\frac{(I-I_0)}{I_o}\times 100$$

where $I_0$ represents the initial current and $I$ is the real-time measured current. Because the dopamine is very sensitive with outdoor light, the measurement was processed in blackout box with blackout curtain. Also, DA solution vials were commonly wrapped with parafilm and aluminum foil to protect them from the harsh environment such as light and humidity.

**Instruments:** Transmission electron microscopy (TEM) and high-resolution TEM (HR-TEM) images were obtained with JEOL JEM–200CX and JEOL JEM–3010 microscopes, respectively. A JEOL 6700 instrument was used to acquire field-effect scanning electron microscopy (FE-SEM) images. X-ray photoelectron spectra (XPS) were recorded using an Axis-His (KRATOS) instrument.

## REFERENCES AND NOTES

(1) Freeman, R.; Elbaz, J.; Gill, R.; Zayats, M.; Willner, I. Analysis of Dopamine and Tyrosinase Activity on Ion-Sensitive Field-Effect Transistor (ISFET) Devices. *Chem. – Euro. J.* **2007**, *13*, 7288-7293

(2) Li, B. R.; Hsieh, Y. J.; Chen, Y. X.; Chung, Y. T.; Pan, C. Y.; Chen, Y. T. An Ultrasensitive Nanowire-Transistor Biosensor for Detecting Dopamine Release from Living PC12 Cells under Hypoxic Stimulation. *J. Am. Chem. Soc.* **2013**, *135*, 16034-16037

(3) Lin, C. H.; Hsiao, C. Y.; Hung, C. H.; Lo, Y. R.; Lee, C. C.; Su, C. J.; Lin, H. C.; Ko, F. H.; Huang, T.-Y.; Yang, Y.-S. Ultrasensitive detection of dopamine using a polysilicon nanowire field-effect transistor. *Chem. Commun.* **2008**, 5749-5751

(4) Feng, X.; Zhang, Y.; Yan, Z.; Chen, N.; Ma, Y.; Liu, X.; Yang, X.; Hou, W. Self-Degradable Template Synthesis of Polyaniline Nanotubes and their High Performance in the Detection of Dopamine. *J. Mater. Chem. A* **2013**, *1*, 9775-9780

(5) Liu, S.; Yu, B.; Zhang, T. Preparation of Crumpled Reduced Graphene Oxide-Poly(p-phenylenediamine) Hybrids for the Detection of Dopamine. *J. Mater. Chem. A* **2013**, *1*, 13314-13320

(6) Chan, E. C. Y.; Wee, P. Y.; Ho, P. Y.; Ho, P. C. High-Performance Liquid Chromatographic Assay for Catecholamines and Metanephrines using Fluorimetric Detection with Pre-Column 9-Fluorenylmethyloxycarbonyl Chloride Derivatization. *J. Chromatogr. B: Biomed. Sci. Appl.* **2000**, *749*, 179-189

(7) Hows, M. E. P.; Lacroix, L.; Heidbreder, C.; Organ, A. J.; Shah, A. J. High-Performance Liquid Chromatography/Tandem Mass Spectrometric Assay for the Simultaneous Measurement of Dopamine, Norepinephrine, 5-Hydroxytryptamine and Cocaine in Biological Samples. *J. Neurosci. Methods* **2004**, *138*, 123-132

(8) Castilho, T. J.; Sotomayor, M. D. P. T.; Kubota, L. T. Amperometric Biosensor Based on Horseradish Peroxidase for Biogenic Amine Determinations in Biological Samples. *J. Pharm. Biomed. Anal.* **2005**, *37*, 785-791

(9) Stoica, L.; Lindgren-Sjölander, A.; Ruzgas, T.; Gorton, L. Biosensor Based on Cellobiose Dehydrogenase for Detection of Catecholamines. *Anal. Chem.* **2004**, *76*, 4690-4696

(10) Lee, J. S.; Jun, J.; Shin, D. H.; Jang, J. Urchin-like Polypyrrole Nanoparticles for Highly Sensitive and Selective Chemiresistive Sensor Application. *Nanoscale* **2014**, *6*, 4188-4194

(11) Lee, J. S.; Kim, S. G.; Jun, J.; Shin, D. H.; Jang, J. Aptamer-Functionalized Multidimensional Conducting-Polymer Nanoparticles for an Ultrasensitive and Selective Field-Effect-Transistor Endocrine-Disruptor Sensors. *Adv. Funct. Mater.* **2014**, *24*, 6145-6153

(12) Shin, D. H.; Lee, J. S.; Jun, J.; Kim, S. G.; Jang, J. Detection of Hazardous Gas Using Multidemensional Porous Iron Oxide Nanorods-Decorated Carbon Nanoparticles. *ACS Appl. Mater. Interfaces* **2015**, *7*, 1746-1751

(13) Jun, J.; Lee, J. S.; Shin, D. H.; Jang, J. Aptamer-Functionalized Hybrid Carbon Nanofiber FET-Type Electrode for a Highly Sensitive and Selective Platelet-Derived Growth Factor Biosensor. *ACS Appl. Mater. Interfaces* **2014**, *6*, 13859-13865

(14) Kim, Y. H.; Kim, K. Y.; Choi, Y. R.; Shim, Y. S.; Jeon, J. M.; Lee, J. H.; Kim, S. Y.; Han, S.; Jang, H. W. Ultrasensitive Reversible Oxygen Sensing by using Liquid-Exfoliated $MoS_2$ Nanoparticles. *J. Mater. Chem. A* **2016**, *4*, 6070-6076

(15) Cho, S.; Kwon, O. S.; You, S. A.; Jang, J. Shape-controlled Polyaniline Chemiresistors for High-Performance DMMP Sensors: Effect of Morphologies and Charge-Transport Properties. *J. Mater. Chem. A* **2013**, *1*, 5679-5688

(16) Holdcroft, S. Patterning π-Conjugated Polymers. *Adv. Mater.* **2001**, *13*, 1753-1765

(17) Geissler, M.; Xia, Y. Patterning: Principles and Some New Developments. *Adv. Mater.* **2004**, *16*, 1249-1269

(18) Lu, X.; Xia, Y. Electronic Materials: Buckling Down for Flexible Electronics. *Nat. Nanotechnol.* **2006**, *1*, 163-164

(19) Cavallo, F.; Turner, K. T.; Lagally, M. G. Facile Fabrication of Ordered Crystalline-Semiconductor Microstructures on Compliant Substrates. *Adv. Funct. Mater.* **2014**, *24*, 1730-1737

(20) Wang, S.; Liu, N.; Tao, J.; Yang, C.; Liu, W.; Shi, Y.; Wang, Y.; Su, J.; Li, L.; Gao, Y. Inkjet Printing of Conductive Patterns and Supercapacitors using a Multi-Walled Carbon Nanotube/Ag Nanoparticle Based Ink. *J. Mater. Chem. A* **2015**, *3*, 2407-2413

(21) Cho, J.; Shin, K. H.; Jang, J. Polyaniline Micropattern onto Flexible Substrate by Vapor Deposition Polymerization-Mediated Inkjet Printing. *Thin Solid Films* **2010**, *518*, 5066-5070

(22) Cho, J.; Shin, K. H.; Jang, J. Micropatterning of Conducting Polymer Tracks on Plasma Treated Flexible Substrate using Vapor Phase Polymerization-Mediated Inkjet Printing. *Synth. Met.* **2010**, *160*, 1119-1125

(23) Shin, K. H.; Cho, J.; Jang, J.; Jang, H. S.; Park, E. S.; Song, K.; Kim, S. H. Polypyrrole Top-Contact Electrodes Patterned by Inkjet Printing Assisted Vapor Deposition

Polymerization in Flexible Organic Thin-Film Transistors. *Org. Electron.* **2012**, *13*, 715-720

(24) Xie, J.; Zhang, Q. Recent Progress in Rechargeable Lithium Batteries with Organic Materials as Promising Electrodes. *J. Mater. Chem. A* **2016**, *4*, 7091-7106

(25) Xu, D.; Xiao, X.; Cai, J.; Zhou, J.; Zhang, L. Highly Rate and Cycling Stable Electrode Materials Constructed from Polyaniline/cellulose Nanoporous Microspheres. *J. Mater. Chem. A* **2015**, *3*, 16424-16429

(26) Liu, J.; Yang, S.; Li, F.; Dong, L.; Liu, J.; Wang, X.; Pu, Q. Highly Fluorescent Polymeric Nanoparticles Based on Melamine for Facile Detection of TNT in Soil. *J. Mater. Chem. A* **2015**, *3*, 10069-10076

(27) Zhao, J.; Wu, G.; Hu, Y.; Liu, Y.; Tao, X.; Chen, W. A Wearable and Highly Sensitive CO Sensor with a Macroscopic Polyaniline Nanofiber Membrane. *J. Mater. Chem. A* **2015**, *3*, 24333-24337

(28) Salavagione, H. J.; Díez-Pascual, A. M.; Lázaro, E.; Vera, S.; Gómez-Fatou, M. A. Chemical Sensors Based on Polymer Composites with Carbon Nanotubes and Graphene: The Role of the Polymer. *J. Mater. Chem. A* **2014**, *2*, 14289-14328

(29) Huang, T. Y.; Kung, C. W.; Wei, H. Y.; Boopathi, K. M.; Chu, C. W.; Ho, K. C. A High Performance Electrochemical Sensor for Acetaminophen Based on a rGO-PEDOT Nanotube Composite Modified Electrode. *J. Mater. Chem. A* **2014**, *2*, 7229-7237

(30) Yu, C.; Choi, K.; Yin, L.; Grunlan, J. C. Light-Weight Flexible Carbon Nanotube Based Organic Composites with Large Thermoelectric Power Factors. *ACS Nano* **2011**, *5*, 7885-7892

(31) Afonso, M.; Morgado, J.; Alcácer, L. Inkjet Printed Organic Electrochemical Transistors with Highly Conducting Polymer Electrolytes. *J. Appl. Phys.* **2016**, *120*, 165502

(32) Xia, Y.; Sun, K.; Ouyang, J. Solution-Processed Metallic Conducting Polymer Films as Transparent Electrode of Optoelectronic Devices. *Adv. Mater.* **2012**, *24*, 2436-2440

(33) Macdiarmid, A. G.; Epstein, A. J. The Concept of Secondary Doping as Applied to Polyaniline. *Synth. Met.* **1994**, *65*, 103-116

(34) Liang, Y.; Li, Y.; Wang, H.; Zhou, J.; Wang, J.; Regier, T.; Dai, H. $Co_3O_4$ Nanocrystals on Graphene as a Synergistic Catalyst for Oxygen Reduction Reaction. *Nat. Mater.* **2011**, *10*, 780-786

(35) Kim, K. S.; Zhao, Y.; Jang, H.; Lee, S. Y.; Kim, J. M.; Kim, K. S.; Ahn, J. H.; Kim, P.; Choi, J. Y.; Hong, B. H. Large-scale Pattern Growth of Graphene Films for Stretchable Transparent Electrodes. *Nature* **2009**, *457*, 706-710

(36) Huang, X.; Qi, X.; Boey, F.; Zhang, H. Graphene-based Composites. *Chem. Soc. Rev.* **2012**, *41*, 666-686

(37) Cao, H.; Zhou, X.; Deng, W.; Liu, Z. A Compressible and Hierarchical Porous Graphene/Co Composite Aerogel for Lithium-ion Batteries with High Gravimetric/Volumetric Capacity. *J. Mater. Chem. A* **2016**, *4*, 6021-6028

(38) Huang, L.; Pan, Y.; Pan, L.; Gao, M.; Xu, W.; Que, Y.; Zhou, H.; Wang, Y.; Du, S.; Gao, H. J. Intercalation of Metal Islands and Films at the Interface of Epitaxially Grown Graphene and Ru(0001) Surfaces. *Appl. Phys. Lett.* **2011**, *99*, 163107

(39) Shin, D. H.; Lee, J. S.; Jun, J.; An, J. H.; Kim, S. G.; Cho, K. H.; Jang, J. Flower-like Palladium Nanoclusters Decorated Graphene Electrodes for Ultrasensitive and Flexible Hydrogen Gas Sensing. *Scientific Reports* **2015**, *5*, 12294

(40) Kundu, P.; Nethravathi, C.; Deshpande, P. A.; Rajamathi, M.; Madras, G.; Ravishankar, N. Ultrafast Microwave-Assisted Route to Surfactant-Free Ultrafine Pt Nanoparticles on Graphene: Synergistic Co-reduction Mechanism and High Catalytic Activity. *Chem. Mater.* **2011**, *23*, 2772-2780

(41) Si, Y.; Samulski, E. T. Exfoliated Graphene Separated by Platinum Nanoparticles. *Chem. Mater.* **2008**, *20*, 6792-6797

(42) Lee, J. S.; Oh, J.; Kim, S. G.; Jang, J. Highly Sensitive and Selective Field-Effect-Transistor NonEnzyme Dopamine Sensors Based on Pt/Conducting Polymer Hybrid Nanoparticles. *Small* **2015**, *11*, 2399-2406

(43) Hu, S.; Huang, Q.; Lin, Y.; Wei, C.; Zhang, H.; Zhang, W.; Guo, Z.; Bao, X.; Shi, J.; Hao, A. Reduced Graphene Oxide-Carbon Dots Composite as an Enhanced Material for Electrochemical Determination of Dopamine. *Electrochim. Acta* **2014**, *130*, 805-809

(44) Wang, Y.; Li, Y.; Tang, L.; Lu, J.; Li, J. Application of Graphene-modified Electrode for Selective Detection of Dopamine. *Electrochem. Commun.* **2009**, *11*, 889-892

(45) Li, S. J.; He, J. Z.; Zhang, M. J.; Zhang, R. X.; Lv, X. L.; Li, S. H.; Pang, H. Electrochemical Detection of Dopamine using Water-Soluble Sulfonated Graphene. *Electrochim. Acta.* **2013**, *102*, 58-65

(46) Gao, F.; Cai, X.; Wang, X.; Gao, C.; Liu, S.; Gao, F.; Wang, Q. Highly Sensitive and Selective Detection of Dopamine in the Presence of Ascorbic acid at Graphene Oxide Modified Electrode. *Sens. Actuators, B* **2013**, *186*, 380-387

(47) Xu, T. T.; Zhu, J.; Yuan, C.; Yang, Q. L.; Cui, K.; Li, C. H.; Wei, L. H.; Ma, Z. New Polymethylene-b-poly(styrene-co-2-hydroxyethyl methacrylate) and Polymethylene-b-

poly(styrene-co-2-hydroxyethyl methacrylate)-g-poly(ε-caprolactone)) Copolymers: Synthesis, Characterization and their Application in the Fabrication of Highly Ordered Porous Films. *Eur. Polym. J.* **2014**, *54*, 109-117

(48) Cho, S.; Hwang, S. H.; Kim, C.; Jang, J. Polyaniline Porous Counter-Electrodes for High Performance Dye-Sensitized Solar Cells. *J. Mater. Chem.* **2012**, *22*, 12164-12171

**Table of contents**